Research Article | Vol. 10, No. 5 | 1 May 2019 | BIOMEDICAL OPTICS EXPRESS 2478
Biomedical Optics EXPRESS

# Spectral complexity of 5-ALA induced PpIX fluorescence in guided surgery: a clinical study towards the discrimination of healthy tissue and margin boundaries in high and low grade gliomas

**L. Alston,[1] L. Mahieu-Williame,[1] M. Hebert,[2] P. Kantapareddy,[3] D. Meyronet,[3,4] D. Rousseau,[1] J. Guyotat,[3] and B. Montcel[1,*]**

[1]*Univ Lyon, INSA-Lyon, Université Lyon 1, UJM-Saint Etienne, CNRS, Inserm, CREATIS UMR5220, U1206, F-69616, Lyon, France*
[2]*Univ Lyon, UJM-Saint-Etienne, CNRS, Institut d Optique Graduate School, Lab. Hubert Curien UMR5516, F-42023, St Etienne, France*
[3]*Hospices Civils de Lyon, Groupe Hospitalier Est, Service d'anatomopathologie, 59 Bvd Pinel, 69394, Lyon, Cedex, France*
[4]*Department of Cancer Cell Plasticity, Cancer Research Centre of Lyon, INSERM U1052, CNRS UMR5286, Lyon, France, Université Claude Bernard Lyon 1, Lyon, France*
**bruno.montcel@creatis.insa-lyon.fr*

**Abstract:** Gliomas are diffuse and hard to cure brain tumors. A major reason for their aggressive behavior is their property to infiltrate the brain. The gross appearance of the infiltrative component is comparable to normal brain, constituting an obstacle to extended surgical resection. 5-ALA induced PpIX fluorescence measurements enable gains in sensitivity to detect infiltrated cells, but still lack sensitivity to get accurate discrimination between the tumor margin and healthy tissue. In this fluorescence spectroscopic study, we assume that two states of PpIX contribute to total fluorescence to get better discrimination of healthy tissues against tumor margins. We reveal that fluorescence in low-density margins of high-grade gliomas or in low-grade gliomas is mainly influenced by the second state of PpIX centered at 620 nm. We thus conclude that consideration of the contributions of both states to total fluorescence can help to improve fluorescence-guided resection of gliomas by discriminating healthy tissues from tumor margins.



## 1 Introduction

Diffuse gliomas account for more than fifty percent of primitive brain tumors and are currently hardly curable. All subtypes share the same highly infiltrative behavior of individual tumor cells. However surrounding infiltrated tissue often resemble normal tissues. The world health organization (WHO) classifies gliomas in 4 grades [1], but most studies commonly consider two separate groups having different biological, molecular and tissue properties: High Grade Gliomas (HGG) and Low Grade Gliomas (LGG). HGG are mainly malignant tumors (grades III and IV of WHO classification), while LGG are benign tumors (grades I and II). In both groups, infiltrative tumor cells are still difficult to identify during surgery. Studies have shown that in 85% cases, recurrences of HGG are localized less than 2 centimeters from the first tumor [2]. Improving the extent of resection prooved to prevent recurrence and improve life quality as well as life expectancy [3–5].

Pre-operative MRI combined with neuro-navigation is currently used to localize surgical tools and tumor cells in the operating theater [6,7] but it shows strong limitations. Indeed, MRI lacks sensitivity to detect tumor margins [8,9]. Furthermore, the brain shift can reach up to 3 cm in comparison with pre-operative MR images [10]. In order to prevent any

#354566 https://doi.org/10.1364/BOE.10.002478
Journal © 2019 Received 17 Dec 2018; revised 9 Feb 2019; accepted 21 Mar 2019; published 18 Apr 2019

Biomedical Optics EXPRESS

localization error due to the brain shift, intraoperative MRI has been suggested. Nonetheless, intraoperative MRI complicates the surgery and has the inherent lacks of sensitivity of MRI to detect tumor margins, which makes it barely used.

As a complementary method to pre-operative MRI, fluorescence microscopy has shown its relevance in neuro-oncology [11–15] and 5-aminolevulonic acid (5-ALA) induced fluorescence of protoporphyrin IX (PpIX) is currently used through surgical microscopes [16]. PpIX takes part in the biosynthesis of heme and ingestion of 5-ALA, precursor in heme's biosynthesis, leads to temporary enhancement of PpIX concentration in gliomas [17]. PpIX absorbs light around 405 nm and emits a reddish fluorescence with a main peak centered at around 634 nm. PpIX fluorescence-guided resection of gliomas through surgical microscopes enabled to gain 6 months life expectancy for HGG [18]. This technique is the actual clinical standard for PpIX-based surgical assistance. It is also investigated for intracranial stereotactic biopsies [19,20]. However, its sensitivity is still limited when applied to low density infiltrative parts of HGG [21,22] or to LGG [23]. Some studies also emphasize that the link between the subjective fluorescence intensity scale chosen by the surgeon and the pathological status of tissues is still to be clarified [24,25].

To overcome sensitivity issues, various 5-ALA induce PpIX fluorescence spectroscopy methods have been proposed. These studies could be classified into two main approaches, either assessing quantitative concentration of PpIX, or qualitative or semi-quantitative biomarkers related to PpIX fluorescence. Quantification of PpIX concentration has been proposed with combined measurements of fluorescence spectroscopy and reflectance to correct tissue distortions [26,27]. This technique is more sensitive than fluorescence microscopy for HGG [28]. It has also been used in LGG but its sensitivity is yet only up to 45% [29]. Some works proposed normalization procedures or other qualitative or semi-quantitative biomarkers to increase the robustness of PpIX fluorescence measurement [19,30–32]. It should be pointed out that both approaches are relevant because all these measurements are intermediary steps toward the final aim of PpIX fluorescence measurements, which is the classification of measurements into relevant pathological status.

Quantification techniques rely on the assumption that the emitted PpIX fluorescence intensity is proportional to the concentration of PpIX. This is supported by the link between the fluorescence emitted intensity and the tumor cellular density [17,33,34]. However, some studies showed more complex links between the PpIX concentration and the shape of fluorescence spectra. A study on biopsies from 5 patients suggests a wavelength shift of the peak intensity of the emitted spectrum in a tumor and nontumor regions [31]. Another study on biopsies raised the presence of two states of PpIX with different fluorescence spectra, peaking at 634 nm and also at 620 nm, in HGG as well as in LGG [32].

The presence of the second peak of fluorescence of PpIX at 620 nm is known in solution and closely linked with the chemical microenvironment [35–38]. This peak has been observed in tissues [32,39–41] or in cell culture [42,43]. But its origin *in vivo* is still an open issue. Some works support the assumption that the origin of the peak at 620 nm *in vivo* is a different aggregate of PpIX [32,42]. Other works [39,43] explained it by precursors of uroporphyrins or coproporphyrins.

The present study aims at investigating the presence of the second peak of fluorescence of PpIX at 620 in non-extracted and freshly extracted living brain tissues, and its correlation with the pathological status of tissues. To do so, we conducted a feasibility clinical trial on 10 patients. An intra-operative fluorescence spectroscopy system has been developed to measure fluorescence spectra of tissues with different pathological status, from healthy tissues to tumor, in HGG and LGG. The complexity of the fluorescence spectra has been investigated by a fitting process considering the two states of PpIX, peaking at 634 nm and also at 620 nm. This led to the definition of new biomarkers of PpIX fluorescence emission, which rely on the concentration of both states of PpIX. These results suggest that these biomarkers could increase the sensitivity of the 5-ALA induced PpIX fluorescence in low density margins and

Biomedical Optics EXPRESS

also to the discrimination of the boundary between tumor margin and healthy tissues in HGG and also in LGG.

## 2. Materials and methods

### 2.1 Patient selection

The study was led at the neurologic center of the Pierre Wertheimer hospital in Bron, France. 10 patients were included in the study, 6 presenting a high-grade glioma and 4 presenting a low-grade glioma.

All experiments were approved by the French Agency for Health (ANSM) and local ethics committee of Lyon University Hospitals (France). All participating patients signed written consent. Inclusion criteria were age equal to or older than 18 years; preoperative diagnosis of LGG or HGG based on clinical signs and enhancement contrast MRI; tumor judged suitable for open cranial resection; and patient ability to provide written consent. Exclusion criteria included pregnancy or breastfeeding; history of cutaneous photo sensitivity or hypersensitivity to porphyrins; photodermatosis, exfoliative dermatitis, or porphyria; history of liver disease within the last 12 months; alanine aminotransferase, aspartate aminotransferase, alkaline phosphatase, or bilirubin levels greater than 2.5 times the normal limit at any time during the previous 2 months; plasma creatinine in excess of 180 µmol/L; patient inability to comply with the photosensitivity precautions associated with the study; and serious associated psychiatric illness. Preoperative, high-resolution contrast-enhanced T1- and/ or T2-weighted axial magnetic resonance images were acquired and used for navigational guidance.

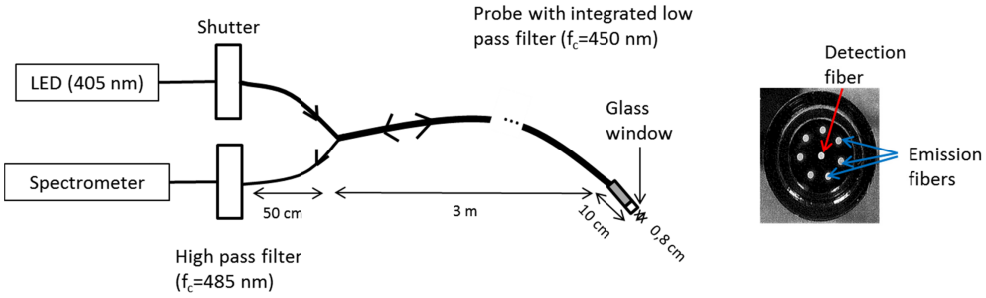


Fig. 1. Drawing of the setup with a picture of the end of the probe.

### 2.2 Spectroscopic setup

The developed device had to be user friendly, efficient and safe. Figure 1 shows a drawing of the setup that is composed of a personal computer offering a Labview interface to drive the system, a box containing electrical and optical components and a probe that is set on the brain to excite the fluorophores and collect fluorescence from tissues. Excitation was performed through a light emitting diode (LED) centered at 405 nm with a 7 nm Full-Width Half-Maximum (M405F1, Thorlabs). Light was transmitted through an optical fiber (HCG M0600T, sedi-fibres) to a probe developed for this study by IDIL company, France.

The characterization of the system is crucial and has been performed on calibrated phantoms in a previous study [37]. We used a fixed concentration of PpIX inspired by the standardization suggested by [44] to demonstrate the ability of the system to measure PpIX fluorescence spectra with both PpIX states.

The inner diameter of the probe is 5 mm and the external diameter is 8 mm, voluntarily close to current surgery tools. A 2 cm thick glass window enables to set the optical fibers always at the same distance of the brain, the probe being directly set on the brain. Inside the probe, exciting light was transmitted through 7 excitation fibers of 600 µm diameter that are

Biomedical Optics EXPRESS

cleaved so that excited tissue area and emitting tissue area are the same. Light goes through a low pass filter with a rejection band between 450 nm and 700 nm. This led to an output irradiance of 30 W/m$^2$. Light was collected through the same probe, with a detection fiber (600 µm diameter) that is placed in the center. Light is then sent to a high pass filter with an in-band transmission between 485 nm and 1200 nm. The filtered light was finally injected into a spectrometer (Maya2000, Ocean optics).

Sterilization of the probe was performed by autoclave process, as recommended by French laws. This implies a steam cycle reaching 134°C and a relative variation of pressure of + 2 bars and −1 bar. Prion risk was tackled with a manual cleaning with an ALKA100 solution (Alkapharm).

### 2.3 Surgical procedure and data acquisition

Patients were given an oral dose of 20 mg/kg of body weight of 5 amino-levulinic acid (Gliolan; Medac GmBH) approximately 3 hours prior to the induction of anesthesia. The patient's head was prepared and registered using a StealthStation Treon image-guidance system (Medtronic) following standard practice. A Zeiss OPMI Pentero surgical microscope (Carl Zeiss Surgical GmbH) modified for fluorescence guidance with a 400-410 nm wavelength source for excitation and a 620-710 nm bandpass filter to record fluorescence emissions on a sensitive 3-chip CCD camera was also coregistered with the surgical field.

For each patient, standard surgical procedure started in order to expose the expected tissue. When asked by the surgeon, surgical procedure was stopped and fluorescence study started. Visual fluorescence was evaluated through surgical microscope. Then, the probe was placed on the tissue to be analyzed, light of the room were lowered and *in vivo* spectroscopic measurements started. Each acquisition was composed of 200 ms of duration with the LED turned on followed by the same duration with the LED turned off to get rid of ambient light coming from the operating room. For each measurement, 12 acquisitions were led, giving a total acquisition time of 4.8 s. The tissue was then removed from the brain and a new measurement was performed on the biopsy (named "*ex vivo* measurement" thereafter) before sending it for histopathological analysis. These fluorescence measurements were performed 6 to 8 times per patient at various stages of surgery. Since the goal of this study is to address the critical stage of minimum visible residual tumor, most of the samples were chosen at the sensitivity limits of the surgical microscope and MR images or beyond them.

In total, 174 measurements were performed and 143 were kept in this analysis. 31 measurements were removed either because they showed no detected fluorescence signal, or due to heterogeneous pathological status, or due to failure to comply with part of the procedure.

### 2.4 Histopathology

Histopathological analysis was performed on formalin fixed paraffin embedded biopsy tissue specimens processed for HES staining. Each H & E stained tissue section was assessed for the presence of tumor cells, necrosis, mitotic activity, nuclear atypia, microvascular proliferation and reactive astrocytosis. Molecular criteria were also assessed. Biopsy specimens were then classified according to WHO histopathological and molecular criteria [1]. Samples were sorted into 5 groups according to their histopathological appearance: HGG solid part, HGG margin, HGG margin of low density, LGG and healthy tissue. Samples classified as "heterogeneous" i.e containing morphological aspects of 2 different categories by the pathologist were removed from the study.

### 2.5 Data pre-processing

For each measurement (*in vivo* or *ex vivo*) of each analyzed tissue, emission spectra was obtained as follow: i) each 'off' spectrum was subtracted from the previous 'on' spectrum to get 12 fluorescence spectra ii) the 12 spectra were summed up to obtain 1 emitted spectrum

Biomedical Optics EXPRESS

per measurement iii) The emitted spectrum was low pass filtered by a zero phase squared cardinal sine window whose width corresponds to the spectrometer's real optical spectral resolution (4 nm).

Autofluorescence of the tissue, mainly NADH, was then removed with a decreasing exponential model, as detailed in Ref [32]. This exponential was automatically sought between two intervals where PpIX fluorescence is negligible. The beginning of the first interval was defined by finding the maximum of the spectrum in the 480-520 nm range, the end of the interval was fixed to 528 nm. The second interval was fixed in the 950-1100 nm range. In order to compare inter- and intra-patient, each spectrum was normalized by the mean value between 520 nm and 528 nm of the autofluorescence model curve. Spectra for which the autofluorescence is non-existent were removed from the study.

### *2.6 Parametric data analysis*

After normalization by autofluorescence, each spectrum was fitted assuming that total fluorescence is a linear combination of the fluorescence emission of three fluorophores in the range 585-640 nm and 950 –11000 nm [32,37,45] as illustrated in Fig. 2. The tissue sample of this figure is a low-density margin of a HGG of a 55-year-old patient. The three fluorophore are the two states of PpIX as introduced previously [32,37] and lipofuscin. The total fit model is defined by the following equation:

$$S(\lambda) = \alpha_{620} S_{620}(\lambda) + \alpha_{634} S_{634}(\lambda) + A_{lipo} \exp\left(-\frac{(\lambda - \lambda_{lipo})^2}{2\sigma_{lipo}^2}\right) \qquad (1.1)$$

where $\alpha_i$ includes all the contributions of the fluorescence intensity of State i (its concentration, quantum yield, molecular extinction coefficient, the incident intensity, the system geometry…), $S_i(\lambda)$ is the reference spectrum of State i (620 or 634) described below, and $A_{lipo}$, $\lambda_{lipo}$ and $\sigma_{lipo}$ are the well-known parameters of the Gaussian curve.

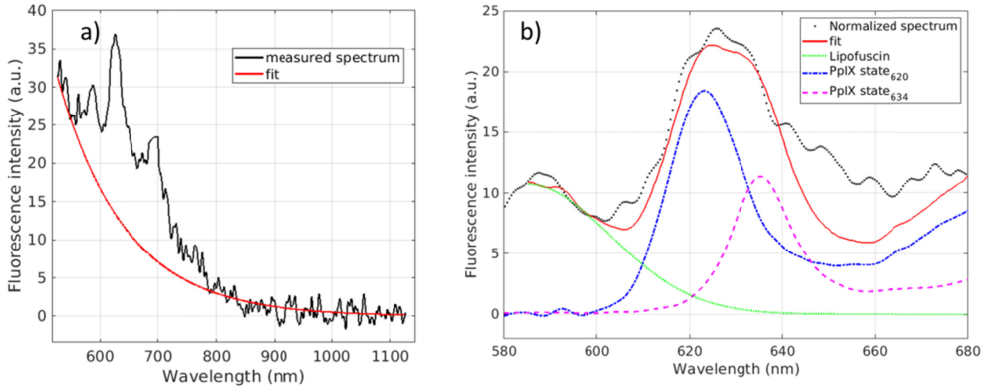


Fig. 2. Data processing: removing of autofluorescence (a) and fit of PpIX and lipofuscin contribution (b). Experimental data (solid black line), fit (solid red curve), normalized spectrum by the autofluorescence (dotted black line), lipofuscin (solid green line), State 620 (dotted blue) and State 634 (dotted purple) measured in a low density margin of a patient aged 55 years old presenting an high grade glioma.

The reference spectra of both PpIX states $S_i(\lambda)$ were measured in aqueous solution as described in Ref [37]. and were normalized by their total fluorescence intensities. Both references were divided by the maximum value of $S_{634}(\lambda)$ for comparison purpose. Due to spectrometer resolution and wavelength shift of the emitted spectra of the two states depending on the microenvironment [32,37], spectra are left free to shift by +/– 2 nm from the reference to reach the best goodness of fitting. Due to fluorescence emission shape

Biomedical Optics EXPRESS

variability of lipofuscin, $\lambda_{lipo}$ and $\sigma_{lipo}$ are left free to adjust, respectively in the 585-600 nm range, and 1-150 nm range to reach the goodness of fitting. As the fit range begins at 585 nm, the lipofuscin function can be considerate to be a half-Gaussian as proposed by [46].

### *2.7 Signal to noise ratio*

We addressed the feasibility of using $\alpha_i$ in a classification process into relevant pathological status. However, we have a low number of samples, and measurements were unequally noisy due to different measurement conditions for the different patients. Then, we decided to measure two signal-to-noise ratios (SNR), $SNR_{620}$ and $SNR_{634}$, where each contribution $\alpha_i$ is divided by the standard deviation of the noise measured at the end of the spectrum, in the 930-1030 nm range, far away from any signal.

## 3. Results

The lipofuscin magnitude appears higher in the *ex vivo* spectra than in the *in vivo* ones whereas the proportion of the two states of PpIX was similar in the both cases. Then all *in vivo* and *ex vivo* measurements have been considered together in these results.

### *3.1 Contributions of both states of PpIX*

One objective of this study is to investigate the relevance of studying two states of PpIX. Thus, Fig. 3 shows the mean value and standard error of the contribution of each state returned by the fit (i.e. $\alpha_i$ normalized by autofluorescence) grouped in the pathological classes: HGG solid part (red star); HGG margins (purple diamond); HGG margins of low density (blue square); LGG (grey circle); and healthy tissue (green triangle). Note that healthy tissues coming from patients with a HGG and a LGG were gathered.

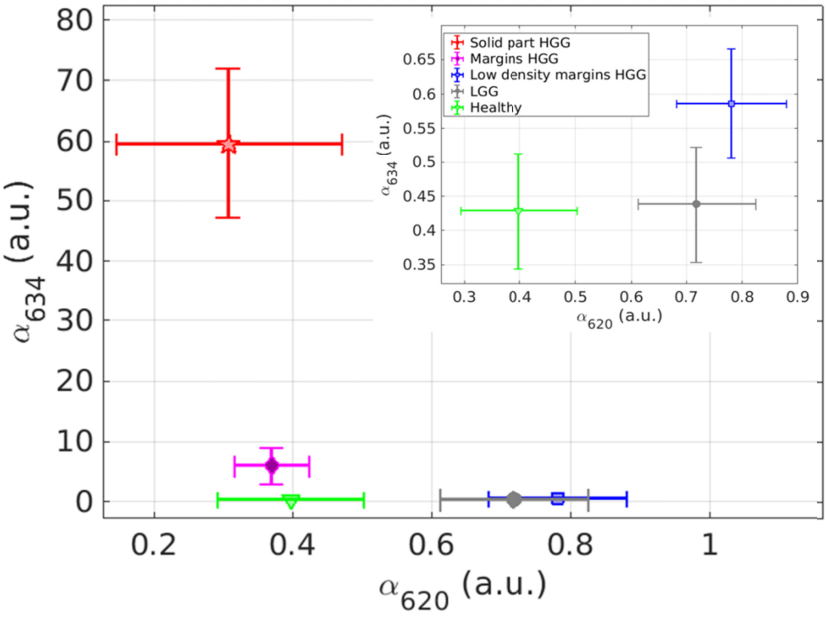


Fig. 3. Mean and standard error of State 634 contribution versus the ones of State 620 for each class: HGG solid part (red star); HGG margins (purple diamond) HGG margins of low density (blue square), LGG (grey circle) and healthy tissues (green triangle). Insert at the top right is a zoom for the low values of state 634.

Results in Fig. 3 show three distinct groups. The first one is the HGG solid part that can be grouped with the HGG margins because the average contribution of the state 634 is really higher than the one of the state 620 in both histopathological classes (more than one order of

Biomedical Optics EXPRESS

magnitude). The second one is the HGG low density margins and LGG where the mean contribution of the state 620 is slightly higher than the one of the state 634. The third group is the healthy tissues where the mean contributions of each state are almost equal and the total contribution of the two states is lower than the other groups. Table 1 displays the numerical values featured in Fig. 3 as well as PpIX fluorescence intensity, evaluated by integrating the fluorescence fitted curve between 600 and 650 nm, and central wavelength of the fluorescence spectrum in the same range. The central wavelength was defined to be the average wavelength of the interval representing more than 80% of the maximum's fluorescence intensity.

**Table 1. mean value and standard error of estimated biomarkers: fluorescence intensity between 600 nm and 650 nm; Central wavelength and contribution of each state.**

| Results | HGG solid part | HGG margins | HGG low density margins | LGG | Healthy |
|---|---|---|---|---|---|
| Fluorescence intensity 600-650 nm (au) | 2362.0 +/– 483.5 | 251.4 +/– 119.9 | 48.9 +/– 6.6 | 45.7 +/– 6.4 | 30.0 +/– 6.2 |
| Central wavelength (nm) | 634.8 +/– 0.2 | 633.2 +/– 0.6 | 629.0 +/– 0.5 | 627.1+/– 0.8 | 633.4 +/– 1.5 |
| Contribution of State 634 (au) | 59.62+/– 12.37 | 5.99 +/– 3.06 | 0.59+/– 0.08 | 0.44 +/– 0.08 | 0.43 +/– 0.08 |
| Contribution of State 620 (au) | 0.31 +/– 0.16 | 0.37 +/– 0.05 | 0.78 +/– 0.10 | 0.72 +/– 0.11 | 0.40 +/– 0.10 |

Table 1 confirms the decrease of total fluorescence intensity when the concentration of tumor cells decreases for HGG, with one to two orders of magnitude of fluorescence intensity higher in solid part of HGG (~2300) than in the others classes (between 30 and 250). Comparing the central wavelength, a shift to lower wavelengths (from 635 nm to 629 nm) appears with decreasing concentration of tumor cells for HGG, as exposed by [31]. The central wavelength value appears to be lower for LGG and HGG low density margins than the others. Finally, the contribution of State 634 decreases from 59 to 0.43 as the concentration of tumor cells decreases, while the contribution of State 620 increases from 0.31 to 0.72, apart for healthy tissues where contributions of the two states are low.

### *3.2 Ratio of the two contributions*

The ratio of the two contributions ($\alpha_{620}$/ $\alpha_{634}$) is drawn on Fig. 4 for each state. This ratio was computed in order to compare it with previous results on biopsies [32]. This ratio tends to 0 in solid parts of HGG and increases as the density of tumor cell decreases. In HGG low density margin and LGG the ratio is higher than 1 and reach around 1.5 in LGG, showing the preponderance of State 620 in LGG. However, this ratio decrease and tends to 1 in healthy tissues.

Biomedical Optics EXPRESS

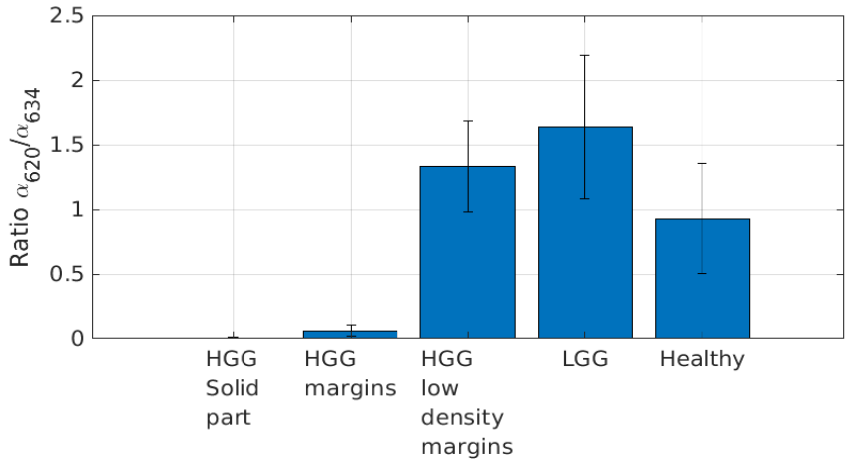


Fig. 4. Ratio of the contribution of State 620 over the one of State 634 for each class.

### *3.3 Signal to noise ratio*

Results above are based on the contribution of each state returned from the fit. Derived biomarkers are the signal-to-noise ratios of each state, $SNR_{634}$ and $SNR_{620}$, either for HGG (Fig. 5) and for LGG (Fig. 6). Dotted line shows the equality of both SNR contributions. We separated HGG and LGG in these figures because the SNR are given for a purpose of classification process into relevant pathological status. Indeed, this process does not imply a classification of LGG versus HGG but only a classification of samples of the same and already defined grade of the glioma. This grade is defined by the preoperative diagnosis.

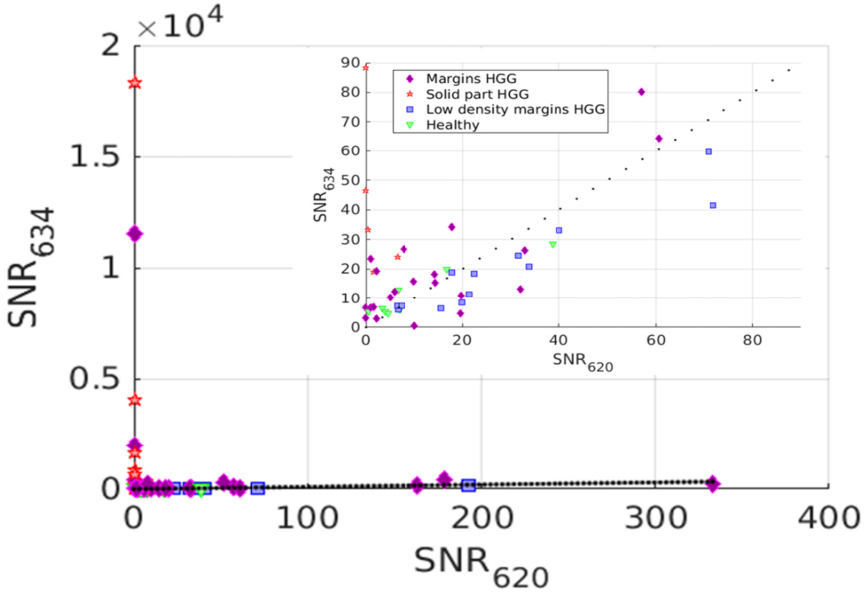


Fig. 5. $SNR_{634}$ versus $SNR_{620}$ for HGG, with a zoom. Markers indicate anatomo-histopathological classification: solid part of HGG (red stars), HGG margins (orange diamonds), HGG margins with low density of tumor cells (blue squares) and healthy tissues (green triangles). Dotted line shows the equality of both SNR contributions.

Biomedical Optics EXPRESS

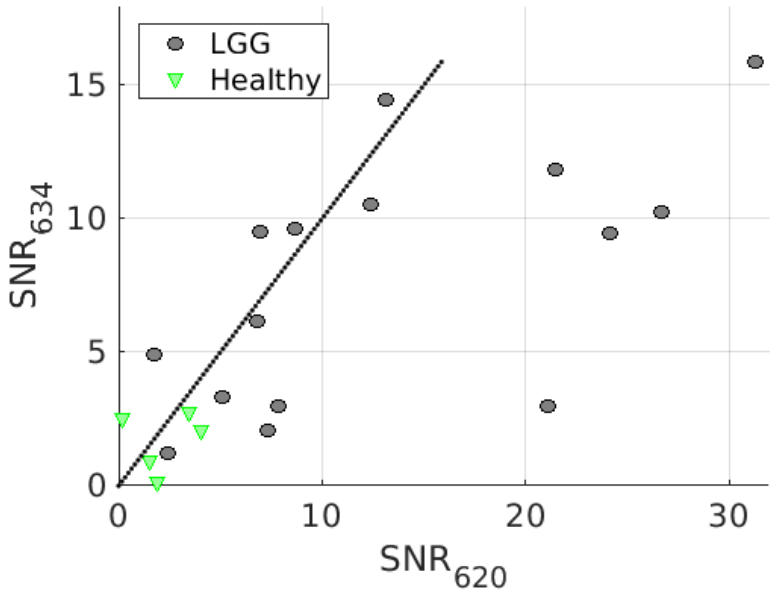


Fig. 6. $SNR_{634}$ versus $SNR_{620}$ for LGG. Markers reveal anatomo-histopathological classification: LGG (black circles) and healthy tissues (green triangle). Dotted line shows the equality of both SNR contributions.

Figure 5 confirms that HGG solid part has an overwhelming contribution of $SNR_{634}$ and almost no contribution of $SNR_{620}$. Most of the HGG margins are above the equal contribution line (dotted line) showing a preponderance of $SNR_{634}$. Whereas the HGG low density margins are below this line, showing a preponderance of $SNR_{620}$. Healthy tissues from the HGG patients are more unequally spread but seem to concentrate in the low SNR of both states region. This figure indicates clearly a different behavior for these four different pathological classes. However, the number of measurements is too low to investigate the statistical relevance of this assumption. This remark is even more striking with the patients of LGG of the Fig. 6. Indeed, the LGG samples have SNR values clearly higher than healthy tissues, even though, as for HGG, no statistical tests support this assumption.

## 4. Discussion

This study confirms the predominance *in vivo* of the commonly studied State 634 of PpIX in the tumor cells high-density regions of HGG (solid part and margin classes) where the ratio ($\alpha_{620}/\ \alpha_{634}$) is close to 0. It is not the case in low-density tumor cells regions (low-density margin of HGG and LGG) where this ratio is higher than 1.

### *4.1 Low PpIX fluorescence intensity in low-density tumor cells regions*

The contribution of state 634 is 10 to 100 times higher in high-density tumor cells regions as compared to healthy or low density tumor cells regions. This should be related to the actual sensitivity issues of the 5-ALA induced PpIX fluorescence surgical microscopy in the low density margin of HGG [21,22] and in LGG [23]. Surgical microscopy fluorescence intensity was also assessed in this study. Data, not shown here, confirm that samples with fluorescence detected with the microscope are mainly localized in high-density tumor cells regions where the contribution of State 634 widely dominates. Quantification of PpIX concentrations is more sensitive than fluorescence microscopy but also shows sensitivity issues in low density tumor cells regions in HGG [28] or LGG [29].These techniques rely on the assumption that the emitted PpIX fluorescence intensity is proportional to the concentration of PpIX. This is

supported by the link between the fluorescence emitted intensity and the tumor cellular density [33,34]. However, some studies show that the microenvironment could have an important role in the intensity of fluorescence. Indeed, a strong 5-ALA induced fluorescence intensity has been observed in a patient showing only inflammatory cells without tumor cells [47]. Furthermore, PpIX accumulation is known to be sensitive to gene expression [48] or metabolic pathways [49]. Our study shows the predominance of State 620 of PpIX in these low-density tumor cells regions. It also shows that the contribution of State 620 is twice higher in these low-density tumor cells regions as compared to healthy and high-density tumor cells regions. It should be pointed that the fluorescence quantum yield of the two aggregates of PpIX are very different, the one of State 634 being far higher than the one of State 620 [36]. Then, a decrease in fluorescence intensity might not only reveal a decrease in PpIX concentration but also a change of PpIX aggregate, in favor of State 620 [37]. Our results suggest that the decrease of PpIX fluorescence intensity in low-density tumor cells regions [21–23] attributed mainly to low PpIX concentrations could also be linked to a different aggregation of PpIX in these regions, due to a microenvironment favoring the PpIX State 620. The similarities in the PpIX fluorescence behaviors in LGG and HGG low density margins could be explained by biological processes rather close from each other: presence of infiltrative but not joined tumor cells without blood brain barrier breakage around.

### *4.2 Towards a discrimination between healthy tissues and margins*

This study shows the low contribution of both states of PpIX in healthy tissues, which is consistent with previous study showing low PpIX concentration [17,27,50]. The contribution of State 634 is constant in healthy tissues and in LGG, and increases of only 37% in low density margin of HGG. This is consistent with the actual sensitivity issues of the 5-ALA induced PpIX fluorescence surgical microscopy in HGG and LGG [21–23]. However, the contribution of State 620 is 80% higher in LGG and 95% higher in low density margins of HGG than in healthy tissues. This opens new insights in the use of this technique during HGG and LGG neurosurgery to discriminate healthy tissues from margins.

### *4.3 Blue shift of PpIX fluorescence spectrum in low-density tumor cells regions*

Table 1 shows a shift of the central wavelength of emitted spectra towards short wavelengths when the density of tumor cells decreases. This shift is almost of 6 nm for low-density tumor cell margins of HGG and even 8 nm in LGG. A study on biopsies also suggests a shift in the same direction of the peak intensity of the emitted spectrum when the density of tumor cells decreases [31], but with a lower magnitude of around 2 nm ± 2 nm. However, in this latter study the wavelength shift was investigated in a margin sample. Then, it is consistent with the shift from high to low density in our study, which was 4 nm. The presence of a second peak of fluorescence at 620 nm, which produces this shift, has been shown in tissues [32,39–41] or in cell culture [42,43]. It is known that such a shift can be induced by a change in PpIX aggregation, which modifies the proportions in State 634 and State 620 of PpIX [35–38]. Hence, the blue shift measured in this study in low-density cell tumor region is another indication that HGG margins and LGG could produce a different aggregation of PpIX, due to a microenvironment favoring State 620 of PpIX.

### *4.4 Ratio of PpIX contributions*

Our previous study explored the ratio of the two contributions of PpIX in HGG and LGG, and showed significant difference between the solid part and margins of HGG [32]. The present study explores this ratio with more precision according to the tumor cell density in tissues. In HGG, the ratio in high density margins is very close to the ratio in the solid part. The significant difference is between the high-density to low-density tumor cell regions, where the ratio reaches values higher than 1. It seems that the relevance of the ratio to discriminate tissues status would rather be in the high to low density transition, instead of solid part to

Biomedical Optics EXPRESS

margin transition as was suggested earlier [32]. In LGG, the ratio is very close to the one observed on low-density tumor cells region of HGG. This confirms the similar PpIX fluorescence behavior that seems to appear in LGG and low-density tumor cell region of HGG, as discussed above. In healthy tissues, the ratio is close to 1. Its relevance to discriminate healthy tissues from margins has to be investigated further.

### *4.5 Origin of the fluorescence peak at 620 nm in vivo*

The presence of the second peak of fluorescence of PpIX at 620 nm is known in solution and closely linked with the chemical microenvironment [35–38]. In particular, PpIX is known to be pH related [32]. The state 620 of PpIX is favored by high pH and the state 634 is favored by low pH. Our results show that the fluorescence peak at 620 nm is preponderant in low-density tumor cells regions; whereas the fluorescence peak at 634 nm is preponderant in high-density tumor cells regions. This can be related to higher acidity in high-density tumor cells regions of HGG as compared to low-density tumor cells regions of HGG and in LGG since it is known that the tumor tissues acidity is correlated to the grade of glioma because of high glycolytic activity [18]. This tends to suggests that the peak at 620 nm is due to a different aggregate of PpIX. However, this study did not retrieve a preponderance of either states of PpIX in healthy tissues. In particular, the contribution of state 620 is not higher than the one of state 634, which would be consistent with the hypothesis of a high pH stated above. Moreover, PpIX is lipophilic; *in vivo*, its distribution is mainly intra-mitochondrial and PpIX is in contact with the lipid membrane of mitochondria, so its microenvironment is quite complex. Furthermore, some results indicate that in ALA-induced and tumor conditions PpIX could spread outside the mitochondria and be partly sensitive to cytosolic microenvironment [51]–[53], or even to extracellular microenvironment [51]. Some works support the assumption that the origin of the peak at 620 nm *in vivo* is a different aggregate of PpIX [32,42]. Other works [39,43] explained it by precursors of uroporphyrins or coproporphyrins. This point is still controversial and should be explored, but it is out of the scope of this study.

### *4.6 Towards classification biomarkers in HGG and LGG*

We investigated the relevance of simple biomarkers, the SNR, directly extracted from this data set with the idea of going towards a classification process into relevant pathological status. It should be emphasized that this is only preliminary work to evaluate the relevance of this way. We separated HGG and LGG, but this process does not imply a classification of LGG versus HGG. The grade of glioma is evaluated before the surgery by other means. We used the same four classes for HGG and two classes for LGG as the one used before in this study. This classification is rather subjective and dependent on the histopathologist. Indeed, we sampled a continuous process (density of tumor cells) that can induce a bias. In HGG, Fig. 5 shows the solid part along the state 634 axis and clearly distincts it from the other groups. The low density and high density margins groups are also distinct from each other, with a separation line which arises from the equal contributions line. Finally, the healthy tissues group seems somehow mixed with the margins groups, but the low contributions are apparent. In LGG, Fig. 6 shows a clear distinction between LGG and healthy tissue. Some studies emphasize the fact that the link between the subjective fluorescence intensity scale chosen by the surgeon in fluorescence microscopy and the pathological status of tissues is still to be clarified [24,25]. Furthermore, classification based on fluorescence of PpIX is used in LGG but show lower sensitivity and specificity [29] than in HGG. Then our results seems rather different, showing that classification based on state 634 and state 620 could highly improve the intraoperative classification efficiency.

### *4.7 Model of fluorescence emission*

The fluorescence emission model used in the parametric data analysis has been discussed previously in detail [32,37]. However further improvements are added in these study with the

Biomedical Optics EXPRESS

fitting of lipofuscin. Lipofuscin concentration is known to be localized around the nucleus of neuronal cells, and its fluorescence emission spectrum shape is known to be linked with aging, oxidation degree and cell stemness degree [46]. The relevance of measuring lipofuscin fluorescence in gliomas can be found in [49] to avoid bias in quantification of the PpIX concentration. Thaw et al [51] presents that fluorescence intensity of Lipofuscin is higher in glial than in glioma cells. As the presence of glioma cells makes glial cell density decrease, the Lipofuscin fluorescence intensity is lower in the solid part or high density margins of the tumor than in heathy tissues and low density margins of the tumor. Data not shown here demonstrate a linear relationship between lipofuscin fitting coefficient and the age of the patient. The oxidation degree has been observed as well since the contribution of lipofuscin appeared to be higher in ex vivo measurements than in *in vivo* ones for an identical sample. Thus lipofuscin fluorescence intensity cannot be neglected in some cases. As the shape of lipofuscin fluorescence is a Gaussian curve and the central wavelength is around 585 nm [11], the contribution of the state 620 is overestimated compared to the one of the state 634 if lipofuscin fluorescence is not extracted. Thus, lipofuscin fluorescence must be extracted to avoid bias in the contributions of both states and between the samples whatever the patient age and the measurement condition (*ex vivo* or *in vivo*).

## 5. Conclusion

In this study, we added the contribution of a second state of PpIX (named State 620) to the well-known and commonly used reference spectra of PpIX (named State 634) to analyze fluorescence spectra of glioma. The goal of this intraoperative clinical trial was to investigate the low sensitivity of fluorescence measurements in low density margins of HGG and LGG and to confirm the power of the second peak of PpIX to help discriminate glioma against healthy tissues. To do so, a linear fitting process was implemented and new biomarkers appeared to be of great interested. Those biomarkers, $\alpha_{620}$ and $\alpha_{634}$ first and then $SNR_{620}$ and $SNR_{634}$ are quick easy to get intraoperatively and could thus help improve fluorescence guided resection of glioma. Indeed, those results confirm that the contribution of State 634 dominates in HGG and their high density margins. What is more, they reveal that the contribution of State 620 is higher than the one of State 634 in low density margins of HGG and in LGG. Blue shift of the central wavelength when the density of tumor cells decreases confirms the weight of State 620 in low density margins. Those results could help understand the lack of sensitivity of current techniques, looking for State 634 where the dominant state is State 620. Based on those two states, the next step is to increase data set and investigated new supervised and unsupervised classification methods to make the discrimination even more robust. Using both states, the discrimination between healthy tissues and regions with a low density of tumor cells appears to be feasible for HGG and LGG as well, offering new opportunities to increase the sensitivity of fluorescence measurements and thus improve the extent of resection and reduce recurrence.

## Funding

French National Research Agency (ANR) (LABEX PRIMES, ANR-11-LABX-0063, Université de Lyon “Investissements d'Avenir” ANR-11-IDEX-0007); Cancéropôle Lyon Auvergne Rhône Alpes (CLARA) (OncoStarter); French National Research Agency (ANR) (France Life Imaging, Infrastructures d’Avenir en Biologie Santé (ANR-11-INBS-000) “Investissements d'Avenir”).

## Acknowledgments

The authors thank the PILoT facility for the support provided on signal acquisition.

## Disclosures

The authors declare that there are no conflicts of interest related to this article.

Biomedical Optics EXPRESS

## References


1. D. N. Louis, A. Perry, G. Reifenberger, A. von Deimling, D. Figarella-Branger, W. K. Cavenee, H. Ohgaki, O. D. Wiestler, P. Kleihues, and D. W. Ellison, "The 2016 World Health Organization Classification of Tumors of the Central Nervous System: a summary," Acta Neuropathol. **131**(6), 803–820 (2016).
2. K. Petrecca, M.-C. Guiot, V. Panet-Raymond, and L. Souhami, "Failure pattern following complete resection plus radiotherapy and temozolomide is at the resection margin in patients with glioblastoma," J. Neurooncol. **111**(1), 19–23 (2013).
3. E. R. Laws, I. F. Parney, W. Huang, F. Anderson, A. M. Morris, A. Asher, K. O. Lillehei, M. Bernstein, H. Brem, A. Sloan, M. S. Berger, and S. Chang; Glioma Outcomes Investigators, "Survival following surgery and prognostic factors for recently diagnosed malignant glioma: data from the Glioma Outcomes Project," J. Neurosurg. **99**(3), 467–473 (2003).
4. Y. M. Li, D. Suki, K. Hess, and R. Sawaya, "The influence of maximum safe resection of glioblastoma on survival in 1229 patients: Can we do better than gross-total resection?" J. Neurosurg. **124**(4), 977–988 (2016).
5. M. Lacroix and S. A. Toms, "Maximum Safe Resection of Glioblastoma Multiforme," J. Clin. Oncol. **32**(8), 727–728 (2014).
6. G. N. Wu, J. M. Ford, and J. R. Alger, "MRI measurement of the uptake and retention of motexafin gadolinium in glioblastoma multiforme and uninvolved normal human brain," J. Neurooncol. **77**(1), 95–103 (2006).
7. N. Sanai, M.-Y. Polley, M. W. McDermott, A. T. Parsa, and M. S. Berger, "An extent of resection threshold for newly diagnosed glioblastomas," J. Neurosurg. **115**(1), 3–8 (2011).
8. C. Senft, A. Bink, K. Franz, H. Vatter, T. Gasser, and V. Seifert, "Intraoperative MRI guidance and extent of resection in glioma surgery: a randomised, controlled trial," Lancet Oncol. **12**(11), 997–1003 (2011).
9. P. L. Kubben, K. J. ter Meulen, O. E. Schijns, M. P. ter Laak-Poort, J. J. van Overbeeke, and H. van Santbrink, "Intraoperative MRI-guided resection of glioblastoma multiforme: a systematic review," Lancet Oncol. **12**(11), 1062–1070 (2011).
10. A. Nabavi, P. M. Black, D. T. Gering, C.-F. Westin, V. Mehta, R. S. Pergolizzi, Jr., M. Ferrant, S. K. Warfield, N. Hata, R. B. Schwartz, W. M. Wells 3rd, R. Kikinis, and F. A. Jolesz, "Serial intraoperative magnetic resonance imaging of brain shift," Neurosurgery **48**(4), 787–797, discussion 797–798 (2001).
11. Y. Li, R. Rey-Dios, D. W. Roberts, P. A. Valdés, and A. A. Cohen-Gadol, "Intraoperative Fluorescence-Guided Resection of High-Grade Gliomas: A Comparison of the Present Techniques and Evolution of Future Strategies," World Neurosurg. **82**(1-2), 175–185 (2014).
12. J. T. C. Liu, D. Meza, and N. Sanai, "Trends in Fluorescence Image-Guided Surgery for Gliomas," Neurosurgery **75**(1), 61–71 (2014).
13. P. A. Valdés, D. W. Roberts, F.-K. Lu, and A. Golby, "Optical technologies for intraoperative neurosurgical guidance," Neurosurg. Focus **40**(3), E8 (2016).
14. R. Maugeri, A. Villa, M. Pino, A. Imperato, G. R. Giammalva, G. Costantino, F. Graziano, C. Gulì, F. Meli, N. Francaviglia, and D. G. Iacopino, "With a Little Help from My Friends: The Role of Intraoperative Fluorescent Dyes in the Surgical Management of High-Grade Gliomas," Brain Sci. **8**(2), 31 (2018).
15. E. D. Bander, R. Magge, and R. Ramakrishna, "Advances in Glioblastoma Operative Techniques," World Neurosurg. **116**, 529–538 (2018).
16. W. Stummer, H. Stepp, G. Möller, A. Ehrhardt, M. Leonhard, and H. J. Reulen, "Technical principles for protoporphyrin-IX-fluorescence guided microsurgical resection of malignant glioma tissue," Acta Neurochir. (Wien) **140**(10), 995–1000 (1998).
17. A. Johansson, G. Palte, O. Schnell, J.-C. Tonn, J. Herms, and H. Stepp, "5-Aminolevulinic Acid-induced Protoporphyrin IX Levels in Tissue of Human Malignant Brain Tumors," Photochem. Photobiol. **86**(6), 1373–1378 (2010).
18. W. Stummer, U. Pichlmeier, T. Meinel, O. D. Wiestler, F. Zanella, and H.-J. Reulen, "Fluorescence-guided surgery with 5-aminolevulinic acid for resection of malignant glioma: a randomised controlled multicentre phase III trial," Lancet Oncol. **7**(5), 392–401 (2006).
19. N. Haj-Hosseini, J. C. O. Richter, P. Milos, M. Hallbeck, and K. Wårdell, "5-ALA fluorescence and laser Doppler flowmetry for guidance in a stereotactic brain tumor biopsy," Biomed. Opt. Express **9**(5), 2284–2296 (2018).
20. B. Kiesel, M. Millesi, A. Woehrer, J. Furtner, A. Bavand, T. Roetzer, M. Mischkulnig, S. Wolfsberger, M. Preusser, E. Knosp, and G. Widhalm, "5-ALA-induced fluorescence as a marker for diagnostic tissue in stereotactic biopsies of intracranial lymphomas: experience in 41 patients," Neurosurg. Focus **44**(6), E7 (2018).
21. J. J. Bravo, J. D. Olson, S. C. Davis, D. W. Roberts, K. D. Paulsen, and S. C. Kanick, "Hyperspectral data processing improves PpIX contrast during fluorescence guided surgery of human brain tumors," Sci. Rep. **7**(1), 9455 (2017).
22. C. G. Hadjipanayis, G. Widhalm, and W. Stummer, "What is the Surgical Benefit of Utilizing 5-Aminolevulinic Acid for Fluorescence-Guided Surgery of Malignant Gliomas?" Neurosurgery **77**(5), 663–673 (2015).
23. M. Jaber, C. Ewelt, J. Wölfer, B. Brokinkel, C. Thomas, M. Hasselblatt, O. Grauer, and W. Stummer, "Is Visible Aminolevulinic Acid-Induced Fluorescence an Independent Biomarker for Prognosis in Histologically Confirmed (World Health Organization 2016) Low-Grade Gliomas?" Neurosurgery (2018).
24. B. Kiesel, M. Mischkulnig, A. Woehrer, M. Martinez-Moreno, M. Millesi, A. Mallouhi, T. Czech, M. Preusser, J. A. Hainfellner, S. Wolfsberger, E. Knosp, and G. Widhalm, "Systematic histopathological analysis of different

Biomedical Optics EXPRESS

5-aminolevulinic acid-induced fluorescence levels in newly diagnosed glioblastomas," J. Neurosurg. **129**(2), 341–353 (2018).
25. E. Belykh, E. J. Miller, A. A. Patel, B. Bozkurt, K. Yağmurlu, T. R. Robinson, P. Nakaji, R. F. Spetzler, M. T. Lawton, L. Y. Nelson, E. J. Seibel, and M. C. Preul, "Optical Characterization of Neurosurgical Operating Microscopes: Quantitative Fluorescence and Assessment of PpIX Photobleaching," Sci. Rep. **8**(1), 12543 (2018).
26. A. Kim, M. Khurana, Y. Moriyama, and B. C. Wilson, "Quantification of in vivo fluorescence decoupled from the effects of tissue optical properties using fiber-optic spectroscopy measurements," J. Biomed. Opt. **15**(6), 067006 (2010).
27. P. A. Valdés, F. Leblond, A. Kim, B. T. Harris, B. C. Wilson, X. Fan, T. D. Tosteson, A. Hartov, S. Ji, K. Erkmen, N. E. Simmons, K. D. Paulsen, and D. W. Roberts, "Quantitative fluorescence in intracranial tumor: implications for ALA-induced PpIX as an intraoperative biomarker," J. Neurosurg. **115**(1), 11–17 (2011).
28. P. A. Valdés, V. L. Jacobs, F. Leblond, B. C. Wilson, K. D. Paulsen, and D. W. Roberts, "Quantitative spectrally resolved intraoperative fluorescence imaging for neurosurgical guidance in brain tumor surgery: pre-clinical and clinical results," in (2014), Vol. 8928, pp. 892809–892809–9.
29. P. A. Valdés, V. Jacobs, B. T. Harris, B. C. Wilson, F. Leblond, K. D. Paulsen, and D. W. Roberts, "Quantitative fluorescence using 5-aminolevulinic acid-induced protoporphyrin IX biomarker as a surgical adjunct in low-grade glioma surgery," J. Neurosurg. **123**(3), 771–780 (2015).
30. N. Haj-Hosseini, J. Richter, S. Andersson-Engels, and K. Wårdell, "Optical touch pointer for fluorescence guided glioblastoma resection using 5-aminolevulinic acid," Lasers Surg. Med. **42**(1), 9–14 (2010).
31. T. Ando, E. Kobayashi, H. Liao, T. Maruyama, Y. Muragaki, H. Iseki, O. Kubo, and I. Sakuma, "Precise comparison of protoporphyrin IX fluorescence spectra with pathological results for brain tumor tissue identification," Brain Tumor Pathol. **28**(1), 43–51 (2011).
32. B. Montcel, L. Mahieu-Williame, X. Armoiry, D. Meyronet, and J. Guyotat, "Two-peaked 5-ALA-induced PpIX fluorescence emission spectrum distinguishes glioblastomas from low grade gliomas and infiltrative component of glioblastomas," Biomed. Opt. Express **4**(4), 548–558 (2013).
33. T. Yoneda, N. Nonoguchi, N. Ikeda, R. Yagi, S. Kawabata, M. Furuse, Y. Hirose, H. Kuwabara, Y. Tamura, Y. Kajimoto, and T. Kuroiwa, "Spectral Radiance of Protoporphyrin IX Fluorescence and Its Histopathological Implications in 5-Aminolevulinic Acid-Guided Surgery for Glioblastoma," Photomed. Laser Surg. **36**(5), 266–272 (2018).
34. S. Kröger, A.-C. Niehoff, A. Jeibmann, M. Sperling, W. Paulus, W. Stummer, and U. Karst, "Complementary Molecular and Elemental Mass-Spectrometric Imaging of Human Brain Tumors Resected by Fluorescence-Guided Surgery," Anal. Chem. **90**(20), 12253–12260 (2018).
35. T. B. Melø and G. Reisaeter, "The physicochemical state of protoporphyrin IX in aqueous solution investigated by fluorescence and light scattering," Biophys. Chem. **25**(1), 99–104 (1986).
36. G. I. Lozovaya, Z. Masinovsky, and A. A. Sivash, "Protoporphyrin IX as a possible ancient photosensitizer: spectral and photochemical studies," Orig. Life Evol. Biosph. **20**(3-4), 321–330 (1990).
37. L. Alston, D. Rousseau, M. Hebert, L. Mahieu-Williame, and B. Montcel, "Nonlinear relation between concentration and fluorescence emission of protoporphyrin IX in calibrated phantoms," J. Biomed. Opt. **23**(9), 1–7 (2018).
38. C. Fuchs, R. Riesenberg, J. Siegert, and R. Baumgartner, "H-dependent formation of 5-aminolaevulinic acid-induced protoporphyrin IX in fibrosarcoma cells," J. Photochem. Photobiol. B **40**(1), 49–54 (1997).
39. M. Zanello, F. Poulon, J. Pallud, P. Varlet, H. Hamzeh, G. Abi Lahoud, F. Andreiuolo, A. Ibrahim, M. Pages, F. Chretien, F. Di Rocco, E. Dezamis, F. Nataf, B. Turak, B. Devaux, and D. Abi Haidar, "Multimodal optical analysis discriminates freshly extracted human sample of gliomas, metastases and meningiomas from their appropriate controls," Sci. Rep. **7**(1), 41724 (2017).
40. W. Dietel, C. Fritsch, R. H. Pottier, and R. Wendenburg, "5-Aminolaevulinic-acid-induced formation of different porphyrins and their photomodifications," Lasers Med. Sci. **12**(3), 226–236 (1997).
41. G. A. Barron, R. Valentine, H. Moseley, L. Brancaleon, C. Hill, and J. A. Woods, "Porphyrin profile in four human cell lines after supplementation with 5-aminolaevulinic acid and its methyl ester," Photodiagn. Photodyn. Ther. **10**(4), 654–663 (2013).
42. C. K. Hope and S. M. Higham, "Evaluating the effect of local pH on fluorescence emissions from oral bacteria of the genus Prevotella," J. Biomed. Opt. **21**(8), 084003 (2016).
43. W. Dietel, R. Pottier, W. Pfister, P. Schleier, and K. Zinner, "5-Aminolaevulinic acid (ALA) induced formation of different fluorescent porphyrins: A study of the biosynthesis of porphyrins by bacteria of the human digestive tract," J. Photochem. Photobiol. B **86**(1), 77–86 (2007).
44. M. Marois, J. Bravo, S. C. Davis, and S. C. Kanick, "Characterization and standardization of tissue-simulating protoporphyrin IX optical phantoms," J. Biomed. Opt. **21**(3), 303003 (2016).
45. D. A. Haidar, B. Leh, M. Zanello, and R. Siebert, "Spectral and lifetime domain measurements of rat brain tumors," Biomed. Opt. Express **6**(4), 1219–1233 (2015).
46. A. C. Croce and G. Bottiroli, "Autofluorescence spectroscopy and imaging: a tool for biomedical research and diagnosis," Eur. J. Histochem. **58**(4), 2461 (2014).
47. K. Omoto, R. Matsuda, I. Nakagawa, Y. Motoyama, and H. Nakase, "False-positive inflammatory change mimicking glioblastoma multiforme under 5-aminolevulinic acid-guided surgery: A case report," Surg. Neurol. Int. **9**(1), 49 (2018).

Biomedical Optics EXPRESS

48. S. Kim, J. E. Kim, Y. H. Kim, T. Hwang, S. K. Kim, W. J. Xu, J.-Y. Shin, J.-I. Kim, H. Choi, H. C. Kim, H. R. Cho, A. Choi, T. Chowdhury, Y. Seo, Y.-S. Dho, J. W. Kim, D. G. Kim, S.-H. Park, H. Kim, S. H. Choi, S. Park, S.-H. Lee, and C.-K. Park, "Glutaminase 2 expression is associated with regional heterogeneity of 5-aminolevulinic acid fluorescence in glioblastoma," Sci. Rep. **7**(1), 12221 (2017).
49. E. Yoshioka, V. S. Chelakkot, M. Licursi, S. G. Rutihinda, J. Som, L. Derwish, J. J. King, T. Pongnopparat, K. Mearow, M. Larijani, A. M. Dorward, and K. Hirasawa, "Enhancement of Cancer-Specific Protoporphyrin IX Fluorescence by Targeting Oncogenic Ras/MEK Pathway," Theranostics **8**(8), 2134–2146 (2018).
50. P. A. Valdés, A. Kim, M. Brantsch, C. Niu, Z. B. Moses, T. D. Tosteson, B. C. Wilson, K. D. Paulsen, D. W. Roberts, and B. T. Harris, "δ-aminolevulinic acid-induced protoporphyrin IX concentration correlates with histopathologic markers of malignancy in human gliomas: the need for quantitative fluorescence-guided resection to identify regions of increasing malignancy," Neuro-oncol. **13**(8), 846–856 (2011).
51. H. H. Thaw, "Optimal conditions for the measurement of lipid peroxidation products (lipofuscin) in individual cultivated human glial and glioma cells," Mech. Ageing Dev. **38**(1), 79–87 (1987).